Towards Global SEM Mantle Convection Simulations on Polyhedral-based Grids

T. N. Phillips[a], J. H. Davies[b], D. Oldham[b,a]

[a]School of Mathematics, Cardiff University, Cardiff CF24 4AG, U.K.
[b]School of Earth and Ocean Sciences, Cardiff University, Cardiff CF10 3AT, U.K.

Abstract

A novel approach to the construction of three-dimensional grids in spherical geometries is described. The grids are based on a range of underlying regular polyhedra. The faces of the polyhedra are arranged into a number of diamonds in the latitudinal and longitudinal directions to facilitate the creation of a structured mesh. Each polyhedron is completely characterized in terms of the arrangement of diamonds. The approach is shown to be very flexible in terms of the meshes that can be generated. It also aids comparisons between the grids used in many mantle convection studies. A spectral element discretization of Poisson's equation is performed to demonstrate the efficacy of the grid generation technique. Rapidly convergent approximations are obtained that demonstrate that fewer degrees of freedom are required to obtain a desired level of accuracy compared with low-order finite element approximations.

Key words: Polyhedral-based grid, mantle convection, spectral element method.

1. Introduction

Although the Earth is an oblate ellipsoid possessing a slight bulge at the equator, the difference between the equatorial and polar radii is sufficiently small (around 21km) that the Earth may be considered as spherical for modelling purposes. Therefore, assuming that the Earth is almost spherical in shape, many problems in Earth Sciences such as mantle convection, ocean and atmosphere modelling and the geodynamo, for example, can be formulated in terms of a system of partial differential equations defined in a spherical geometry. The approach that we have adopted circumvents the

problems associated with perhaps the most intuitive way of discretising a system of equations on the sphere using spherical coordinates that results in the so-called latitude-longitude (lat-long) grid. Although the lat-long grid has some desirable features at low latitude in that it is orthogonal and quasi-uniform, it also possesses some serious computational deficiencies.

Firstly, the spherical polar coordinate system has singularities at the two poles. At these points direction is undefined and the metric is singular. This means that one has to take great care in defining the various differential operators that are required in the formulation of the problem. For example, the gradient operator in spherical polar coordinates is

$$\nabla = \mathbf{e}_r \frac{\partial}{\partial r} + \mathbf{e}_\theta \frac{1}{r} \frac{\partial}{\partial \theta} + \mathbf{e}_\phi \frac{1}{r \sin \theta} \frac{\partial}{\partial \phi}, \tag{1}$$

where $\mathbf{e}_r$, $\mathbf{e}_\theta$ and $\mathbf{e}_\phi$ are unit vectors in the radial, latitudinal and longitudinal directions, respectively. Clearly, alternative representations for the gradient operator are required at the north and south poles since $\sin \theta$ vanishes at those points. These representations are generated using L'Hôpital's rule so that a total of three distinct forms of the gradient operator are required in this coordinate system.

The second problem is a consequence of the convergence of the meridians towards the poles. This creates a far greater density of grid points near the poles and smaller grid spacing in the longitudinal direction in the polar regions. The grid convergence towards the poles imposes a severe restriction on the choice of time step for explicit time integration schemes. This is caused by the metric factor $(r \sin \theta)^{-1}$ in the component of the gradient operator in the $\mathbf{e}_\phi$ direction (see (1)), for example, becoming unbounded near the poles when a uniform grid spacing is used in the longitudinal direction.

There are a number of features that are desirable in a computational mesh on a sphere. These include orthogonality, absence of problems associated with grid convergence and coordinate singularities and a single domain approach to meshing the entire spherical geometry. As far as we are aware it is not possible to construct a mesh that possesses all of these features. As we have seen the lat-long grid fails to meet two of these criteria. The Yin-Yang grid (Tackley, 2008; Yoshida and Kageyama, 2004; Sadourny et al., 1968) sacrifices the last of these criteria. It is based on a decomposition of the sphere into two geometrically identical regions, each of which is symmetric in two perpendicular directions.

The Yin-Yang grid retains some elements of the lat-long structure but removes the 'pole problems' by overlaying two lat-long grids in such a way that the poles of neither are present. This has the advantage in that each component grid is rectangular in computational (θ, ϕ) space and so software that has been developed for the lat-long grid can be adapted for use on this grid. However, the boundary of each of the two component lat-long grids is rather irregular and there is an overlap between the two that needs to be minimized in order to preserve the underlying properties of the yin-yang decomposition. It is probably for this reason that the Yin-Yang grid is normally used in conjunction with finite difference and finite volume approximations.

An alternative grid-based method to the tensor product grid produced by equal mesh spacing in the longitudinal and latitudinal directions is to cover the sphere as uniformly as possible with nodes. The distribution of these nodes can then be used to construct a finite element mesh. The problem of how to distribute points uniformly on the surface of a sphere was posed by Euler as far back as the 18th century. This problem, that can be stated remarkably simply, has not only inspired mathematicians but also attracted the attention of scientists working in fields such as crystallography, molecular structure and electrostatics (Saff and Kuijlaars, 1997). The five Platonic solids provide solutions to the problem. However, the Platonic solid with the largest number of sides is the icosahedron with 12 vertices and 20 equilateral triangles. This is the largest number of vertices that satisfies the property of uniform distribution on a sphere.

To obtain a finer discretization using a larger number of vertices one has to relax the uniform distribution property to obtain a triangulation of the sphere that is almost uniform in some sense. This approach was pioneered by Baumgardner and Frederickson (1985) who constructed a finite element mesh on the sphere using the projection of a regular icosahedron onto the sphere as the starting point. The twelve vertices of the icosahedron define a mesh of twenty identical spherical triangles bounded by thirty geodesic arcs. Subsequent refinements of the grid are obtained by connecting the mid-points of each of the three sides of a spherical triangle by geodesic arcs to obtain four smaller spherical triangles. However, these smaller triangles are not identical which results in a non-uniform triangulation of the sphere at the finer level. Although the triangles are almost of the same size, the triangulation is non-uniform nevertheless with the attendant programming complications and deterioration in accuracy due to mesh irregularity.

The most popular spherical grids that have been used over the last twenty

3

years have been based on the contribution of Baumgardner and Frederickson (1985) (Zhong et al., 2008). Although any polyhedron can be used to create a spherical grid, the most commonly used are the Platonic solids. The Platonic solids possess several important and useful properties viz. the vertices lie on the surface of a sphere, the edges of the faces have the same length and the angles at all vertices at all faces are identical. Platonic solids that are often used include the cube (6 faces) (Komatitsch et al., 2002; Choblet, 2005; Sadourny, 1972) and icosahedron (20 faces) (Baumgardner, 1985; Majewski et al., 2002). An example of a polyhedron that is not a platonic solid that has been used to create a spherical grid is the rhombic dodecahedron (12 faces) (Zhong et al., 2000). Although the vertices of a rhombic dodecahedron do not all lie on the surface of a sphere, they can still be projected onto the surface of a sphere to form the basis for the generation of a spherical grid.

In a recent paper (Oldham et al., 2012), the authors described a flexible approach to the creation of grids on the surface of a sphere based on an underlying polyhedron that may be regular (such as the cube and icosahedron) or irregular (such as the rhombic dodecahedron). The faces of the polyhedra are combined to form diamonds. The diamonds are then used as the basis for the construction of a structured mesh. This grid generation procedure provides increased flexibility in terms of the total number of nodes or degrees of freedom that can be used to describe the system and facilitates comparisons between the grids used in virtually all current mantle convection codes. A range of grids constructed using this software was used to solve Poisson's equation on the surface of a sphere using a spectral element discretization. The spectral element method generates a solution to a system of differential equations by decomposing the computational domain into a number of conforming elements and representing the dependent variables using a basis associated with the Legendre polynomials. This results in a high-order approximation that converges extremely rapidly depending on the smoothness of the solution. The preconditioned conjugate gradient method was used to solve the linear system of equations generated by the discretization. Convergence of the numerical approximation and high-order accuracy were obtained on all of the grids.

In this paper we extend the approach to three-dimensional spherical geometries through the introduction of radial elements. This is a geometry that resembles the domain used in mantle convection studies. The three-dimensional grid generation and the subsequent approximation of the solution of Poisson's equation in a three-dimensional spherical shell of finite

thickness using the spectral element method have been validated.

2. Poisson's Equation in a Spherical Shell

Consider the solution of Poisson's equation

$$-\nabla^2 u = f \tag{2}$$

in the three-dimensional spherical domain Ω defined by

$$\Omega = \{(r, \phi, \theta) : r \in [R_I, R_O], \phi \in [0, 2\pi], \theta \in [0, \pi]\}.$$

where $f \in L^2(\Omega)$ and the Laplacian in spherical polars is defined by

$$\nabla^2 = \frac{1}{r^2} \frac{\partial}{\partial r} \left(r^2 \frac{\partial}{\partial r} \right) + \frac{1}{r^2 \sin^2 \theta} \frac{\partial^2}{\partial \phi^2} + \frac{1}{r^2 \sin \theta} \frac{\partial}{\partial \theta} \left(\sin \theta \frac{\partial}{\partial \theta} \right) \tag{3}$$

Let Γ_I and Γ_O denote the inner and outer boundaries of Ω corresponding to spherical surfaces with $r = R_I$ and $r = R_O$, respectively. Suppose that Dirichlet boundary conditions are imposed on the solution at the inner and outer surfaces of Ω so that

$$u = u_I, \quad \text{on } \Gamma_I, \tag{4}$$
$$u = u_O, \quad \text{on } \Gamma_O. \tag{5}$$

The spectral element method is based on a discretization of the weak formulation of the problem. The trial and test spaces are defined by

$$V = \{v \in H^1(\Omega) : v = u_I \text{ on } \Gamma_1, v = u_O \text{ on } \Gamma_2\},$$

and

$$W = \{v \in H^1(\Omega) : v = 0 \text{ on } \Gamma_1 \cup \Gamma_2\},$$

respectively. The weak formulation of the problem is derived by multiplying (2) by $v \in W$ and integrating over Ω. This yields the weak problem: find $u \in V$ such that

$$a(u, v) = L(v), \quad \forall v \in W,$$

where $a(\cdot, \cdot)$ is the bilinear form defined by

$$a(u, v) = \int_\Omega \left(\frac{\partial u}{\partial r} \frac{\partial v}{\partial r} + \frac{1}{r^2 \sin^2 \theta} \frac{\partial u}{\partial \phi} \frac{\partial v}{\partial \phi} + \frac{1}{r^2} \frac{\partial u}{\partial \theta} \frac{\partial v}{\partial \theta} \right) r^2 \sin \theta \, dr d\theta d\phi,$$

and $L(\cdot)$ is the linear functional given by

$$L(v) = \int_\Omega f \, v \, r^2 \sin \theta \, dr d\theta d\phi.$$

5

3. Computational Grid

The computational grid is constructed in two stages. In the first stage, a spherical grid is created on the surface of the unit sphere. In the second stage this spherical grid is projected onto the surfaces of a number of concentric spheres with radii in the interval $[R_I, R_O]$ to form 3D elements. The starting point is to choose a polyhedron that is to be used as the basis for the construction of a spherical grid. Popular polyhedra that have been used in mantle convection studies include the cube, icosahedron and rhombic dodecahedron.

The polyhedron is divided into a number of diamonds with each diamond comprising either two triangular faces with the property that their common edge is a latitudinal line of symmetry or one rhombic face. The projections of the diamonds onto the sphere are identical spherical parallelograms bounded by four geodesic arcs. Each spherical parallelogram forms a patch on the sphere that can be subdivided into a number of elements. This is achieved by connecting corresponding points on opposite sides of the spherical parallelogram by geodesic arcs. Three-dimensional elements are then formed by projecting these elements onto the surfaces of concentric spheres with radii lying in the interval $[R_I, R_O]$ to obtain spherical tiles.

Many polyhedra can be characterized in terms of the number of diamonds in the latitudinal (N_θ) and longitudinal (N_ϕ) directions (see Fig. 1). The cubed-sphere grid corresponds to the choice $N_\theta = 2$, $N_\phi = 3$. Since each diamond is composed of four sides, it can easily be mapped onto a square array for computational purposes. The simplest configuration has $N_\theta = 1$ and $N_\phi = 3$. Although it is possible, in theory, to construct a computational grid using arbitrarily large values of N_θ and N_ϕ, there are practical reasons why one would not want to do so in practice. For example, for large values of N_θ and N_ϕ the diamonds become increasingly irregular in terms of size and shape particularly near the poles where they become elongated in latitude and near the equator where they become stretched in the longitudinal direction.

Each diamond is uniquely referenced by two indices: $d_\theta \in [1, \ldots, N_\theta]$ in the latitudinal direction and $d_\phi \in [1, \ldots, N_\phi]$ in the longitudinal direction (see Fig. 2). The coordinates of the vertices of each polyhedron on the unit sphere can be expressed in terms of the angles θ and ϕ. The longitudinal coordinate can be found by dividing 2π by the number of diamonds. If ϕ_N, ϕ_E, ϕ_S, ϕ_W denote the longitudinal locations of the vertices at the North, East, South and West corners of the diamond referenced by the pair (d_ϕ, d_θ)
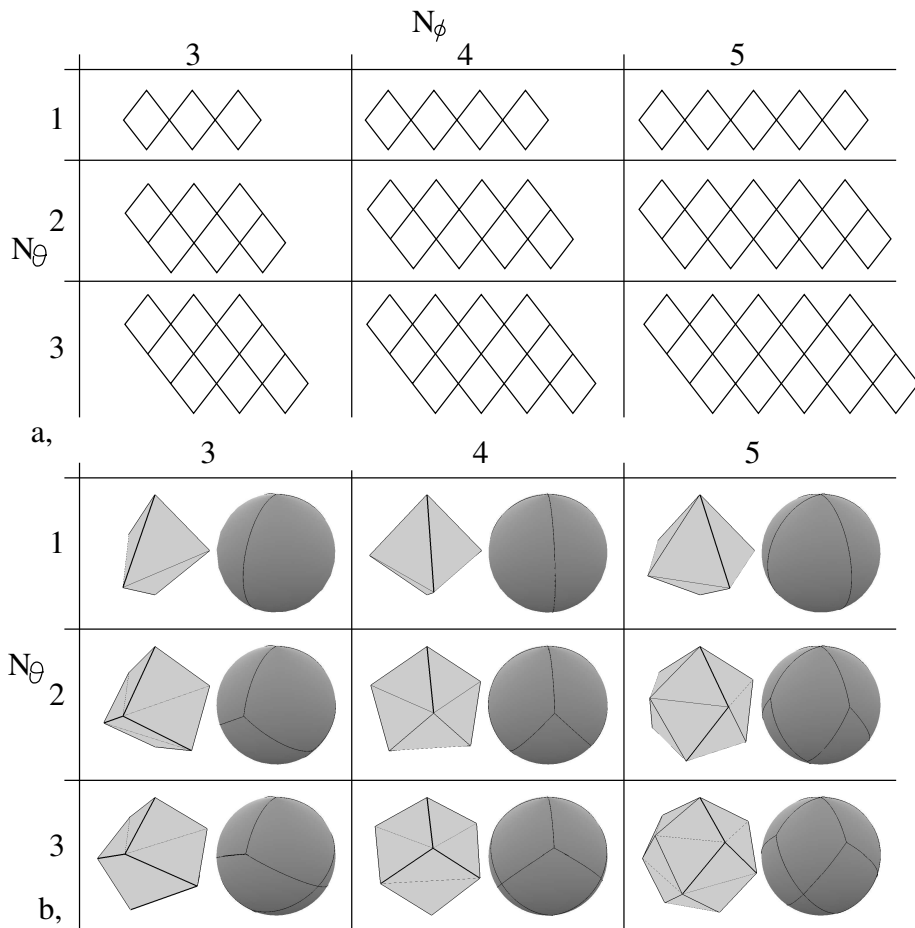
6

Figure 1: The decomposition of several polyhedra into **diamonds**. Each diamond normally contains two triangular faces of the polyhedron. However there are special cases in which the diamonds contain a single rhombic face, e.g. when $N_\theta = 2$, $N_\phi = 3$ (the cube) and $N_\theta = 3, N_\phi = 4$ (the rhombic dodecahedron). (a), Two dimensional representations of a range of polyhedra. (b), Three dimensional images of the polyhedra and the projection of the polyhedron onto the sphere. Note that the images of the polyhedra and their projections are viewed from a point close to the object rather than infinity.

then we have

$$\phi_N = \frac{\pi}{N_\phi}(d_\theta + 2d_\phi - 2)$$

$$\phi_E = \frac{\pi}{N_\phi}(d_\theta + 2d_\phi - 1)$$

$$\phi_S = \frac{\pi}{N_\phi}(d_\theta + 2d_\phi - 2)$$

$$\phi_W = \frac{\pi}{N_\phi}(d_\theta + 2d_\phi - 3)$$

The calculation of the corresponding latitudinal coordinates of the vertices is more complex. For $N_\theta \leq 3$, the vertices are located so that all the triangles in the polyhedron have the same area. If we define α_A to be the angle between the edge connecting the West and East vertices of a given diamond with the edge connecting the West and North (or East and North) vertices then the equal area property (area of unit sphere $= 2\times$ area of spherical triangle $\times$ number of diamonds) requires that

$$\alpha_A = \frac{\pi}{N_\theta N_\phi} + \frac{\pi}{2} - \frac{\pi}{N_\phi}.$$

For polyhedra for which $N_\theta \leq 3$, the latitudinal locations are given by

$$\theta_N = \alpha_A \delta_{d_\theta,2} + \frac{\pi}{2}\delta_{d_\theta,3}$$

$$\theta_E = \alpha_A \delta_{d_\theta,1} + \frac{\pi}{2}\delta_{d_\theta,2}\delta_{N_\theta,3} + (\pi - \alpha_A)\,\delta_{d_\theta,N_\theta}$$

$$\theta_S = \pi\delta_{d_\theta,N_\theta} + (\pi - \alpha_A)\,\delta_{d_\theta+1,N_\theta} + \frac{\pi}{2}\delta_{d_\theta,1}\delta_{N_\theta,3}$$

$$\theta_W = \alpha_A \delta_{d_\theta,1} + \frac{\pi}{2}\delta_{d_\theta,2}\delta_{N_\theta,3} + (\pi - \alpha_A)\,\delta_{d_\theta,N_\theta}$$

where δ is the Kronecker delta. This rather complex approach is adopted to ensure that the polyhedra generated by the diamonds characterized by $N_\theta = 1$, $N_\phi = 4$ (octahedron); $N_\theta = 2$, $N_\phi = 3$ (cube); $N_\theta = 2$, $N_\phi = 5$ (icosahedron); and $N_\theta = 3$, $N_\phi = 4$ (rhombic dodecahedron) are regular.

There are no regular polyhedra for $N_\theta > 3$, and a different approach is adopted. The sphere is decomposed into a number of regions separated by lines of constant latitude on which the vertices of the polyhedra are located. The lines of constant latitude are positioned so that each region has the
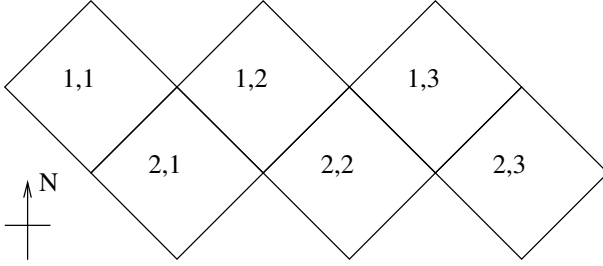
Figure 2: Labelling of the diamonds within an example polyhedron (cube). Each diamond is represented by two numbers: the diamond number in latitude d_1 and longitude d_2 where $d_1 \in [1, N_\phi]$ & $d_2 \in [1, N_\theta]$

same area with the aim of ensuring that the diamonds constructed using this approach have approximately the same area.

Finally, each diamond is divided into a number of elements. Opposite edges of each diamond are partitioned in an identical fashion using the same number of nodes so that there is a total of $K_d = N_t^2$ elements per diamond. Corresponding edge nodes are then connected by geodesic arcs and the intersection of these form the elements. Therefore, there is a rectangular array of elements associated with each diamond. To facilitate continuity of the approximation across elements and also to simplify the data structures, we further assume that this array of elements is square so that there is an identical number of nodes along each diamond edge. If there are N_r radial spherical shells then the total number of elements in Ω is

$$K = N_\theta N_\phi N_t^2 N_r.$$

4. Discrete Weak Formulation

The domain Ω is decomposed into K elements, Ω_k, $k = 1, \ldots, K$, with $\Omega = \cup_{k=1}^{K} \Omega_k$ and $\Omega_i \cap \Omega_j = \emptyset$ for $i \neq j$. Each physical element is mapped onto the parent or reference cube $\Omega_R = [-1, 1]^3$ using a transfinite mapping. In the case of the bilinear form $a(\cdot, \cdot)$ we have

$$
\begin{aligned}
a(u, v) &= \sum_{k=1}^{K} \int_{\Omega_k} \nabla u \cdot \nabla v \, dx^1 dx^2 dx^3 \\
&= \sum_{k=1}^{K} \int_{\Omega_R} g_{ab} \frac{\partial u}{\partial \xi^a} \frac{\partial v}{\partial \xi^b} |J_k| \, d\xi^1 d\xi^2 d\xi^3
\end{aligned}
\tag{6}
$$

9

where the Einstein summation convention has been employed so that the integrand is summed for a, $b = 1, 2, 3$. In this equation J_k is the Jacobian of the mapping from Ω_k to Ω_R and the metric is defined by

$$g_{ab} = \frac{\partial \xi^a}{\partial x^A} \frac{\partial \xi^b}{\partial x^A}. \tag{7}$$

Similarly, the linear functional $L(\cdot)$ is given by

$$L(v) = \sum_{k=1}^{K} \int_{\Omega_R} f v |J_k| \, d\xi^1 d\xi^2 d\xi^3 \tag{8}$$

The mapping of an element onto the parent cube is constructed as follows. Consider a spherical tile element bounded by spherical parallelograms on spheres of radii R_1 and R_2 with $R_1 < R_2$. Each of these spherical parallelograms is a projection of the spherical parallelogram on the surface of the unit sphere defined by vertices with position vectors $\mathbf{X}_i$, $i = 1, \ldots, 4$. Define the blending functions F and G along the great arc connecting the points with position vectors $\mathbf{X}_i$ and $\mathbf{X}_j$ by

$$F(\xi, \alpha_{ij}) = \cos\left(\frac{(1+\xi)}{2}\alpha_{ij}\right) - \frac{\cos(\alpha_{ij})}{\sin(\alpha_{ij})} \sin\left(\frac{(1+\xi)}{2}\alpha_{ij}\right) \tag{9}$$

$$G(\xi, \alpha_{ij}) = \frac{\sin(\frac{1}{2}(1+\xi)\alpha_{ij})}{\sin(\alpha_{ij})} \tag{10}$$

for $\xi \in [-1, 1]$ where
$$\alpha_{ij} = \cos^{-1}(\mathbf{X}_i \cdot \mathbf{X}_j).$$

Next define the mapping

$$\begin{aligned}
\mathbf{X}(\xi^1, \xi^2) = {} & \mathbf{X}_1 F(\xi^1, \alpha_{12}) F(\xi^2, \alpha_{14}) + \mathbf{X}_2 G(\xi^1, \alpha_{21}) F(\xi^2, \alpha_{23}) \\
& + \mathbf{X}_3 G(\xi^1, \alpha_{34}) G(\xi^2, \alpha_{32}) + \mathbf{X}_4 F(\xi^1, \alpha_{43}) G(\xi^2, \alpha_{41})
\end{aligned}$$

This is a one-to-one mapping from the square $[-1, 1]^2$ onto the spherical parallelogram on the unit sphere. Note that

$$|\mathbf{X}(\xi^1, \xi^2)| = 1, \text{ for all } -1 \leq \xi^1, \xi^2 \leq 1.$$

The significance of this is that the mapping provides an exact rather than a polygonal representation of the surface. If we now define a mapping in the radial direction from the interval $[-1, 1]$ onto $[R_1, R_2]$ by

$$R\left(\xi^3\right) = \frac{1}{2}\left(R_2 - R_1\right)\left(1 + \xi^3\right) + R_1, \quad \xi^3 \in [-1, 1]$$

then the full three-dimensional mapping is given by

$$\mathbf{x}(\xi^1, \xi^2, \xi^3) = \mathbf{X}(\xi^1, \xi^2)R\left(\xi^3\right). \tag{11}$$

A knowledge of the mapping (11) enables us to calculate the partial derivatives

$$\frac{\partial x^A}{\partial \xi^b},$$

and thus to calculate the entries of G given by

$$G_{ab} = \frac{\partial x^A}{\partial \xi^a}\frac{\partial x^A}{\partial \xi^b}.$$

The entries of g required in the bilinear form (6) are determined by inverting G. For the mapping given by (11), G is given explicitly by

$$G = \begin{bmatrix} (\frac{\partial X^A}{\partial \xi^1})^2 R^2 & \frac{\partial X^A}{\partial \xi^1}\frac{\partial X^A}{\partial \xi^2}R^2 & 0 \\ \frac{\partial X^A}{\partial \xi^2}\frac{\partial X^A}{\partial \xi^1}R^2 & (\frac{\partial X^A}{\partial \xi^2})^2 R^2 & 0 \\ 0 & 0 & \frac{1}{4}(R_2 - R_1)^2 \end{bmatrix}$$

The determinant of G is

$$|G| = \frac{1}{4}(R_2 - R_1)^2 R^2 \left[\left(\frac{\partial X^A}{\partial \xi^1}\right)^2 \left(\frac{\partial X^A}{\partial \xi^2}\right)^2 - \left(\frac{\partial X^A}{\partial \xi^1}\frac{\partial X^A}{\partial \xi^2}\right)^2 \right]$$

from which one can determine the Jacobian of the mapping

$$J = \sqrt{|G|}.$$

5. Spectral Element Method

The spectral element method (Patera, 1984; Maday and Patera, 1989) is based on the weak formulation of the problem: find $u \in V$ such that

$$a(u, v) = L(v), \ \forall v \in W. \tag{12}$$

Let $V_N \subset V$ denote the discrete solution space. We denote by $\mathrm{P}_N(\Omega_k)$ the space of all polynomials on Ω_k of degree less than or equal to N, and further define

$$P_N(\Omega) = \{\phi : \phi|_{\Omega_k} \in \mathrm{P}_N(\Omega_k)\}$$

The approximation space is defined by

$$V_N = V \cap P_N(\Omega) \tag{13}$$

The approximation on element Ω_k is given by

$$u_N^k(\xi^1, \xi^2, \xi^3) = \sum_{i=0}^{N} \sum_{j=0}^{N} \sum_{k=0}^{N} u_{i,j,k}^k h_i(\xi^1) h_j(\xi^2) h_k(\xi^3). \tag{14}$$

where the Lagrangian interpolants $h_i(\xi)$, $0 \leq i \leq N$, are defined on the parent interval with $\xi \in [-1, 1]$ by the relationship

$$h_i(\xi) = -\frac{(1 - \xi^2) L_N'(\xi)}{N(N+1) L_N(\xi_i)(\xi - \xi_i)}, \tag{15}$$

The Gauss-Lobatto Legendre (GLL) points ξ_i, $i = 0, \ldots, N$, are the zeros of $(1 - \xi^2) L_N'(\xi)$ and $L_N(\xi)$ is the Legendre polynomial of degree N.

The dimension of V_N is denoted by N_V and V_N is spanned by the set of global basis functions $\{\phi_j(\mathbf{x}) : j = 1, \ldots, N_V\}$. If the solution is represented in terms of these basis functions as follows:

$$u_N(\mathbf{x}) = \sum_{j=1}^{N_V} u_j \phi_j(\mathbf{x}) \tag{16}$$

then the linear system associated with the discrete form of (12) is

$$A_N u_N = f_N. \tag{17}$$

12

where the entries of A_N are approximations to

$$A_{i,j} = a(\phi_j, \phi_i)$$

obtained by expressing integrals over Ω as a sum of integrals over Ω_k, $k = 1, \ldots, K$, and approximating these using Gauss-Lobatto Legendre quadrature rules. For example, consider the contribution to the bilinear form (6) by one of the terms in the integrand (corresponding to $a = 1$ and $b = 1$) over one particular element. The approximation to the solution is given by (14) and the test function is of the form

$$v_N(\xi^1, \xi^2, \xi^3) = h_l(\xi^1)h_m(\xi^2)h_n(\xi^3), \quad 0 \le l, m, n \le N. \tag{18}$$

The approximation to the term

$$\int_{\Omega_R} g_{1,1}(\xi^1, \xi^2, \xi^3) \frac{\partial u_N}{\partial \xi^1} \frac{\partial v_N}{\partial \xi^1} |J(\xi^1, \xi^2, \xi^3)| \, d\xi^1 d\xi^2 d\xi^3$$

is then given by

$$\sum_{p=0}^{N} w_p w_m w_n g_{1,1}(\xi_p^1, \xi_m^2, \xi_n^3) |J(\xi_p^1, \xi_m^2, \xi_n^3)| \left(\sum_{i=0}^{N} D_{p,i} u_{i,m,n} \right) D_{p,l}$$

where w_p, $p = 0, \ldots, N$, are the GLL quadrature weights and D is the Legendre differentiation matrix whose entries are given by $D_{ij} = h'_j(\xi_i)$. The explicit expressions for the entries of D are given by

$$D_{j,k} = \begin{cases} \dfrac{1}{(x_j - x_k)} \dfrac{L_N(x_j)}{L_N(x_k)}, & j \ne k, \\[2ex] 0, & 1 \le j = k \le N - 1, \\[2ex] -\dfrac{N(N+1)}{4}, & j = k = 0, \\[2ex] \dfrac{N(N+1)}{4}, & j = k = N. \end{cases}$$

The right-hand side of (17) is obtained by approximating the linear functional $L(\mathbf{v})$ in a similar fashion. Since the matrix A_N is symmetric and positive definite, the linear system (17) can be solved using the preconditioned conjugate gradient method. The preconditioner used is a Jacobi preconditioner.

6. Numerical Results

The spectral element method was used in conjunction with grids generated using projections of several polyhedra described earlier including the cube ($N_\theta = 2$, $N_\phi = 3$), icosahedron ($N_\theta = 2$, $N_\phi = 5$) and rhombic dodecahedron ($N_\theta = 3$, $N_\phi = 4$). Poisson's equation was solved within a spherical shell geometry of finite thickness. A problem with a known non-trivial solution was used to validate the accuracy of the numerical approximation on meshes characterized in terms of N_θ, N_ϕ, K_d and N. More precisely, for each underlying polyhedra used to generate the basic mesh and for $K_d = 1$ and $K_d = 4$, the L^2-norm of the error in the approximation is determined as a function of polynomial order N.

The Poisson equation (2) is solved in the spherical shell domain Ω with right-hand side defined by

$$
\begin{aligned}
f(r,\theta,\phi) \;=\; & \frac{\sin^2\theta}{R^2}\left[(\cos\phi - \sin\phi)\left(20\sin^2\theta - 15\right) - \sin 2\phi\left(10\sin^2\theta - 6\right)\right] \\
& \times \left[\left(\frac{r}{R_I}\right)^2 - 1\right]\left[\left(\frac{r}{R_O}\right)^2 - 1\right] \\
& + \sin^4\theta\left[\cos\phi - \sin\phi - \frac{1}{2}\sin 2\phi\right]\left[\frac{20r^2}{R_I^2 R_O^2} - 6\left(\frac{1}{R_I^2} + \frac{1}{R_O^2}\right)\right]
\end{aligned}
$$

The analytical solution to this problem is given by

$$
u(r,\theta,\phi) = \sin^4\theta\left[\cos\phi - \sin\phi - \frac{1}{2}\sin 2\phi\right]\left[\left(\frac{r}{R_I}\right)^2 - 1\right]\left[\left(\frac{r}{R_O}\right)^2 - 1\right]
$$

This expression is used to generate the Dirichlet boundary conditions on the inner and outer surfaces of Ω. The computations were performed for $R_I = 1$ and $R_O = 3$.
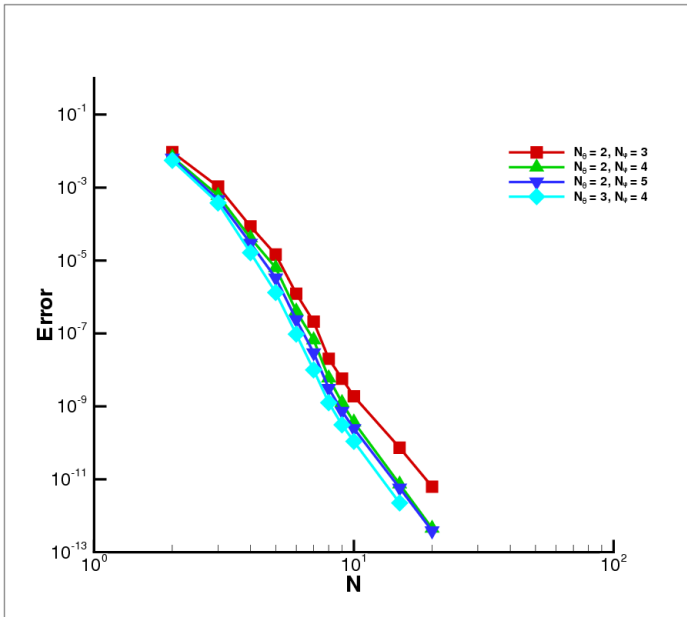
The L^2-norm of the error is given by

$$
\|e\|_2 = \left\{\sum_{k=1}^{K}\sum_{i=0}^{N}\sum_{j=0}^{N} w_i w_j |J_k\left(\xi_i,\eta_j\right)|\left[u_e\left(\xi_i,\eta_j\right) - u\left(\xi_i,\eta_j\right)\right]^2\right\}^{\frac{1}{2}} \tag{19}
$$

where w_i, $i = 0,\ldots,N$ are the Gauss-Lobatto Legendre weights and $|J_k|$ is the determinant of the Jacobian in the kth spectral element Ω_k.
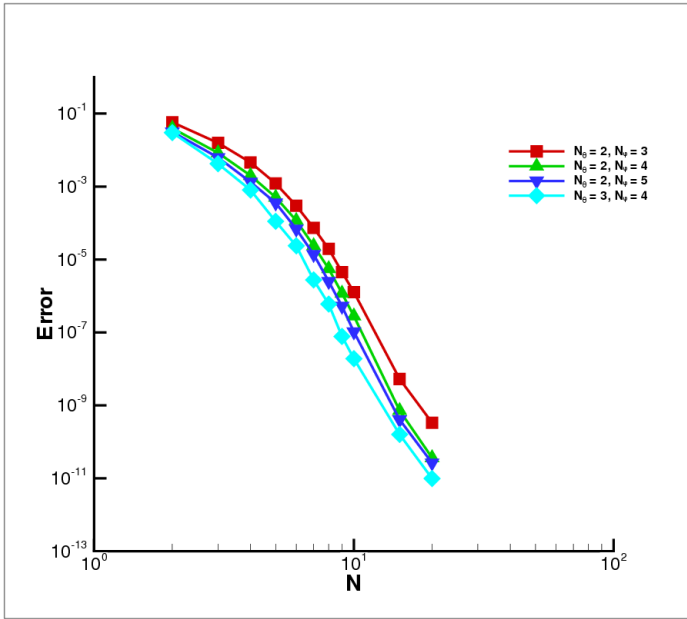
(a)

(b)

Figure 3: The decay of the error (19) for the Poisson problem defined on a spherical shell as a function of the spectral order N: (a) With one SE per diamond ($N_t = 1$) and (b) with 16 SE per diamond ($N_t = 4$).

15

The convergence behaviour in Fig. 3 shows that for $5 \leq N \leq 8$ exhibits algebraic convergence with the error decaying like $O(N^{-14})$. For $N \geq 9$ the rate of convergence slows down slightly but still converges more rapidly than low-order methods such as the finite element method. To quantify this claim consider a quadratic finite element discretisation of the cubed-sphere grid. With a single finite element per diamond this corresponds to the data point for $N = 2$ in Fig. 3(a). The quadratic finite element approximation to the solution of Poisson's equation converges cubically i.e. $O(N^{-3})$. This means that to attain the same error as for the spectral element method with $N = 20$ one would require a level of refinement with in excess of 3,800 grid points in each dimension per spectral element or put another way the total number of degrees of freedom would differ by a factor of over 10^{10}.

Excellent error reduction is obtained on all of the polyhedral grids generated using the approach outlined in this paper. The differences between the decay of the error is minimal for the grids based on the cube, icosahedron and rhombic dodecahedron, especially considering that the number of computational nodes per diamond differs for each polyhedron. More precisely, the grid based on the rhombic dodecahedron possesses more degrees of freedom than the grid based on the cube for a given value of polynomial order N.

7. Conclusions

This paper has presented an approach that generates structured meshes for problems defined in three-dimensional spherical domains without the deficiencies associated with the most intuitive structured mesh viz. the lat-long grid. The foundation of the approach is the decomposition of the faces of a regular polyhedron into diamonds and the projection of the polyhedron onto a sphere. The mesh generation technique is very valuable since it can be used to construct and compare many of the grids that are commonly used in mantle convection studies.

The overall objective of our research programme is to develop and implement the first spherical mantle convection code based on a spectral element discretization of the governing equations. The heart of the problem in terms of computational effort is the solution of a generalized Stokes problem incorporating the momentum equation and the incompressibility constraint. The solution of the Stokes problem requires the inversion of the Poisson operator. In this paper we have developed a spectral element approximation to the solution of Poisson's equation in three-dimensional spherical geometries on

polyhedral-based meshes. Although Dirichlet boundary conditions are implemented in this paper, alternative physically meaningful boundary conditions such as free-slip at the core-mantle boundary can be easily incorporated into the weak formulation. The linear system of equations generated by consideration of the discretization of the weak formulation of the problem was solved using the conjugate gradient method with a diagonal preconditioner.

Acknowledgements

References

Baumgardner, J.R., 1985. Three-dimensional treatment of convective flow in the earth's mantle. Journal of Statistical Physics 39, 501–511.

Baumgardner, J.R., Frederickson, P.O., 1985. Icosahedral discretization of the two-sphere. SIAM J. Numer. Anal. 22, 1107–1115.

Choblet, G., 2005. Modelling thermal convection with large viscosity gradients in one block of the 'cubed sphere'. Journal of Computational Physics 205, 269–291.

Komatitsch, D., Ritsema, J., Tromp, J., 2002. The spectral-element method, beowulf computing, and global seismology. Science 298, 1737–1742.

Maday, Y., Patera, A.T., 1989. Spectral element methods for the incompressible Navier-Stokes equations, in: Noor, A.K., Oden, J.T. (Eds.), State of the Art Surveys in Computational Mechanics. ASME, New York, pp. 71–143.

Majewski, D., Liermann, D., Prohl, P., Ritter, B., Buchhold, M., Hanisch, T., Paul, G., Wergen, W., , Baumgardner, J., 2002. The operational global icosahedral-hexagonal gridpoint model GME: description and high-resolution tests. Monthly Weather Review 130, 319–338.

Oldham, D., Davies, J.H., Phillips, T.N., 2012. Generic polyhedron grid generation for solving partial differential equations on spherical surfaces. Comput. and Geosci. 39, 11–17.

Patera, A.T., 1984. A spectral element method for fluid dynamics: laminar flow in a channel expansion. Journal of Computational Physics 54, 468–488.

Sadourny, R., 1972. Conservative finite-difference approximations of primitive equations on quasi-uniform spherical grids. Monthly Weather Review 100, 136–144.

Sadourny, R., Arakawa, A., Mintz, Y., 1968. Integration of nondivergent barotropic vorticity equation with an icosahedral-hexagonal grid for sphere. Monthly Weather Review 96, 351–356.

Saff, E.B., Kuijlaars, A.B.J., 1997. Distributing many points on a sphere. Math. Intell. 19, 5–11.

Tackley, P., 2008. Modelling compressible mantle convection with large viscosity contrasts in a three-dimensional spherical shell using the yin-yang grid. Physics of the Earth and Planetary Interiors 171, 7–18.

Yoshida, M., Kageyama, A., 2004. Application of the yin-yang grid to a thermal convection of a Boussinesq fluid with infinite Prandtl number in a three-dimensional spherical shell. Geophysical Research Letters 31. Paper number L12609.

Zhong, S., McNamara, A., Tan, E., Moresi, L., Gurnis, M., 2008. A benchmark study on mantle convection in a 3-D spherical shell using CitcomS. Geochemistry Geophysics Geosystems 9. Paper number Q10017.

Zhong, S., Zuber, M., Moresi, L., Gurnis, M., 2000. Role of temperature-dependent viscosity and surface plates in spherical shell models of mantle convection. Journal of Geophysical Research-Solid Earth 105, 11063–11082.